

Machine-Learned Preconditioners for Linear Solvers in Geophysical Fluid Flows

Jan Ackmann¹, Peter D. Düben², Tim N. Palmer¹, Piotr K. Smolarkiewicz³

¹University of Oxford, Oxford, OX1 3PU, UK

²European Centre For Medium Range Weather Forecasts, Reading, RG2 9AX, UK

³National Center for Atmospheric Research, Boulder, CO 80026, USA

Key Points:

- The preconditioning step in linear solvers of weather and climate models can be performed using machine learning.
- The approach can be learned from timesteps and no analytically-derived preconditioner is required as reference.
- The machine-learned preconditioner can be interpreted in order to improve designs of conventional preconditioners.

arXiv:2010.02866v1 [physics.ao-ph] 6 Oct 2020

Corresponding author: Jan Ackmann, jan.ackmann@physics.ox.ac.uk

Abstract

It is tested whether machine learning methods can be used for preconditioning to increase the performance of the linear solver – the backbone of the semi-implicit, grid-point model approach for weather and climate models.

Embedding the machine-learning method within the framework of a linear solver circumvents potential robustness issues that machine learning approaches are often criticized for, as the linear solver ensures that a sufficient, pre-set level of accuracy is reached. The approach does not require prior availability of a conventional preconditioner and is highly flexible regarding complexity and machine learning design choices.

Several machine learning methods are used to learn the optimal preconditioner for a shallow-water model with semi-implicit timestepping that is conceptually similar to more complex atmosphere models. The machine-learning preconditioner is competitive with a conventional preconditioner and provides good results even if it is used outside of the dynamical range of the training dataset.

Plain Language Summary

The recent boom of machine-learning techniques has a huge impact on many areas of science. In this paper, we propose a new approach that is using machine learning in a part of weather and climate models called the dynamical core which is solving the discrete representation of the underlying equations of motion. In particular, we are focussing here on a model component that is required to solve an expensive linear optimisation problem each time-step. When running a model simulation, this part of the model is typically responsible for a large fraction of the computational cost.

We show how machine-learning can be used to speed-up these linear optimisation problems. We study our approach in a representative model of medium complexity that has similar properties when compared to the dynamical core of a full weather or climate model. We describe how the machine-learning approach can be applied, discuss its properties and show the performance in comparison to conventional methods. The approach is successful as it allows for stable simulations with high efficiency that are competitive with conventional model configurations.

1 Introduction

Climate prediction models continue to show systematic deficiencies whose magnitude is comparable with the (e.g. greenhouse gas forcing) signals we seek to simulate and understand (Palmer & Stevens, 2019). In a nonlinear system like climate, such deficiencies compromise the reliability of almost all regional outputs derived from such models. These deficiencies appear to arise from the way in which key physical processes - deep convection, orographic gravity waves and ocean mesoscale eddies in particular - are parameterised rather than modelled directly from the laws of physics. As such, an important goal for the coming years is the development of global climate models where these processes are resolved directly. However, such a goal cannot be achieved simply by relying on next-generation exascale computers - we need also to improve the computational efficiency of existing numerical codes radically. In this paper we address a central component of a broad class of climate models – we target the dynamical core using machine learning.

Machine learning methods show great potential for various applications across the entire workflow of weather and climate modelling including observation pre-processing, data assimilation, forecast models and post-processing. Machine learning is for example used to improve models via the development of new physical parametrisation schemes

(e.g. Schneider et al. (2018); Gentine et al. (2018)) or via emulation of existing parametrisation schemes to improve model efficiency (e.g. Chevallier et al. (1998); Krasnopolsky et al. (2010); Rasp et al. (2018)). Other approaches aim to learn the equations of motion of the atmosphere and the ocean directly – effectively replacing the entire dynamical core (Dueben and Bauer (2018); Scher and Messori (2019); Weyn et al. (2019)). Developing machine learning applications, and in particular deep learning, is highly desirable as they run very efficiently on modern supercomputers. Next-generation supercomputing hardware will be optimised (co-designed) for deep learning applications that use dense linear algebra at low numerical precision – using 16 bits or less to represent real numbers (see for example Kurth et al. (2018)).

This paper aims to improve computational efficiency of the dynamical core by using machine learning to develop preconditioners for linear solvers. Efficient linear solvers are essential for atmosphere and ocean models that are using implicit or semi-implicit timestepping schemes. Implicit schemes revolve around solving a problem in which the flow state at timestep (t^{n+1}) depends non-linearly on information from timestep (t^{n+1}); in contrast to explicit schemes that only use information from current/previous timesteps (t^n, t^{n-1}, \dots); for a recent overview see (Mengaldo et al., 2019). In practice, often semi-implicit timestepping schemes are used which evaluate slow-moving parts of the equations of motion explicitly and solve implicitly for pressure to cover the fast-moving parts. As a result, (semi-)implicit methods allow for the use of much longer timesteps. For example the explicit COSMO model (Fuhrer et al., 2018) uses 12 seconds, at similar resolution the fully-implicit model in (Yang, Xue, et al., 2016) was pushed to an extreme value of 240 seconds – too large timesteps eventually lead to a degradation of model solutions. However, for implicit models the linear solver is responsible for the majority of the computational cost. This paper is focussing on the class of Krylov sub-space methods but the approach presented should also be relevant for multigrid-based methods, see (Müller & Scheichl, 2014; Maynard et al., 2020) for recent publications on linear solvers.

To reduce the cost of the linear solver – which typically requires a number of solver iterations for convergence – efficient preconditioners are essential. A preconditioner directly inverts specific parts of the linear problem in order to significantly reduce the number of solver iterations. However, deriving efficient preconditioners is a difficult exercise requiring substantial research (Müller and Scheichl (2014); Maynard et al. (2020); Kühnlein et al. (2019); Piotrowski et al. (2016); Dedner et al. (2016)). There have been some advances to apply machine-learning methods within the context of linear solvers. So far, work has focused on using machine learning to either select the best solver-preconditioner setup from a set of preconditioners and/or linear solvers for a given linear problem (Holloway & Chen, 2007; Kuefler & Chen, 2008; Xu & Zhang, 2005; George et al., 2008; Yamada et al., 2018; Huang et al., 2016; Peairs & Chen, 2011), to help improve efficiency for Block-Jacobi type preconditioners (Götz & Anzt, 2018), to reduce the time-to-solution by interspersing linear solver iterations with neural-network based correction steps (Rizzuti et al., 2019), or to replace the linear solver entirely (Tompson et al., 2017; Yang, Yang, & Xiao, 2016; Ladický et al., 2015).

This paper will try a fundamentally new approach by using supervised machine learning to derive the preconditioner directly. We will perform preliminary tests and train machine learning preconditioners for the application in a global shallow water model. This specific approach to preconditioning has several advantages. Machine learning methods, and deep learning methods in particular, are often criticised for potentially leading to unphysical model behaviour if the methods are used outside of the dynamic range of the training dataset, for example in a changing climate. The use of machine learning in the preconditioner is, however, not as vulnerable to these problems. If the performance of the machine-learning preconditioner degrades, the linear solver will only continue with the timestep if the error of the solution reaches a user-defined threshold. Also, for the machine-learned preconditioner the complexity of the machine learning method and its

set of input variables can be freely adjusted by the user to performance requirements. This makes the machine-learned preconditioner very flexible, which is important for efficient parallel communication on supercomputers.

Section 2 provides information about the model and the testcase that is used. Section 2.3 describes how machine learning is used to develop preconditioners. Section 3 is presenting the results including the offline performance of machine-learned preconditioners, the use of the preconditioners within free-running simulations, an investigation about the learned properties of the preconditioners, and a brief discussion of computational performance. Section 4 provides a discussion and the conclusion.

2 Model and Test-case

2.1 Shallow-Water Model

We use an Eulerian, semi-implicit shallow-water model that is conceptionally similar to the Finite Volume Model (FVM-IFS) which is developed at the European Centre for Medium-Range Weather Forecasts as a new dynamical core for the Integrated Forecasting System (IFS; P. K. Smolarkiewicz et al. (2016, 2019); Kühnlein et al. (2019)). The shallow-water model is using the well-known MPDATA advection scheme (Prusa et al., 2008; Szmelter & Smolarkiewicz, 2010) and the shallow water equations on the sphere are discretised as defined in (P. K. Smolarkiewicz & Margolin, 1998; Szmelter & Smolarkiewicz, 2010):

$$\frac{\partial G\Phi}{\partial t} + \nabla \cdot (\mathbf{v}\Phi) = 0, \quad (1)$$

$$\frac{\partial GQ_x}{\partial t} + \nabla \cdot (\mathbf{v}Q_x) = GR_x \quad (2)$$

$$\frac{\partial GQ_y}{\partial t} + \nabla \cdot (\mathbf{v}Q_y) = GR_y, \quad (3)$$

where Φ is the fluid thickness, Q_x and Q_y denote the momenta in $x = \lambda$ (longitudinal) and $y = \phi$ (latitudinal) directions. $G \equiv h_x h_y$ is the Jacobian of the geospherical framework, with h_x, h_y being the metric coefficients of the general orthogonal coordinates; here $h_x = a \cos(\phi)$, $h_y = a$ for a lat-lon grid with Earth's radius a . \mathbf{v} is the advective velocity.

The corresponding forcing terms for the momenta in equations (2) and (3) are:

$$R_x = -\frac{g}{h_x} \Phi \frac{\partial(\Phi + H_0)}{\partial x} + fQ_y + \frac{1}{G\Phi} (Q_y \frac{\partial h_y}{\partial x} - Q_x \frac{\partial h_x}{\partial y}) Q_y, \quad (4)$$

$$R_y = -\frac{g}{h_y} \Phi \frac{\partial(\Phi + H_0)}{\partial y} - fQ_x - \frac{1}{G\Phi} (Q_y \frac{\partial h_y}{\partial x} - Q_x \frac{\partial h_x}{\partial y}) Q_x. \quad (5)$$

The terms occurring on the right-hand-sides are, from left to right, the pressure gradient, the Coriolis force, and the metric terms. H_0 is the topography, g the gravitational acceleration and f the Coriolis parameter.

Equations (1)-(3) are discretized in a semi-implicit fashion on a collocated lat-lon grid. While the explicit part of the momentum equations is evaluated via the MPDATA approach (P. K. Smolarkiewicz & Margolin, 1998), this paper is focusing on the linear solver which is used for the implicit part of the time integration. The linear problem to be solved for Φ^{n+1} originates from inserting the trapezoidal integrals of the momentum equations (2) and (3) into the trapezoidal integral of equation (1). It can be symbolically written as:

$$\mathcal{L}(\Phi^{n+1}) - \mathcal{R} = 0. \quad (6)$$

For illustration, \mathcal{R} incorporates the explicit parts of the time integration that were already computed outside of the solver, while \mathcal{L} represents the discretised implicit terms. Here, \mathcal{L} is a linear operator which is negative-definite but not self-adjoint. \mathcal{L} has the form of a generalized Laplacian:

$$\mathcal{L}(\Phi) := \sum_{I=1}^2 \frac{\partial}{\partial x^I} \left(\sum_{J=1}^2 A^{IJ} \frac{\partial \Phi}{\partial x^J} + B^I \Phi \right) - \Phi, \quad (7)$$

with the six coefficient fields: A^{11} (zonal direction), A^{12}, A^{21} (cross-derivative terms), A^{22} (meridional direction), B^1 and B^2 .

After spatially discretising the linear problem (6), it can be solved using a linear solver, here the preconditioned generalized conjugated residual method (GCR; see P. Smolarkiewicz and Margolin (2000); Eisenstat et al. (1983) and flowchart in supporting information), a Krylov subspace method that iteratively minimizes the Euclidean norm of the residual vector r_ν at each solver iteration ν :

$$r_\nu = \mathcal{L}(\Phi_\nu) - \mathcal{R}. \quad (8)$$

The solver is iterated until the infinity norm of the residual is found to be smaller than an ϵ value that is adjusted to application needs $\frac{\|r_\nu\|_\infty}{\|r_0\|_\infty} \leq \epsilon$ (results are qualitatively the same if using the Euclidean norm instead; not shown). If the solver is converged after N iterations, we set $\Phi^{n+1} := \Phi_N$.

We use an ‘implicit Richardson’ preconditioner \mathcal{P} as reference to allow for a qualitative comparison between conventional and machine learning approaches (see supporting information), that is based on performing implicit Richardson iterations in zonal direction to diminish the effects of grid-convergence near the poles. This approach is equivalent to the well-known treatment of the vertical dimension with a tridiagonal solver, see (Müller & Scheichl, 2014; Maynard et al., 2020). The preconditioner has been successfully tested for shallow-water test-cases from the Williamson test-suite (Williamson et al., 1992) and allowed for solver speed-ups of factor 3 to 10 (not shown here).

2.2 Test-case

We apply the model to the zonal geostrophic flow test-case as described in (Williamson et al., 1992) with the parameters $\alpha = 0$, $u_0 = 20 \frac{m}{s}$, and $h_0 = 5960m$. However, to increase the complexity of the test-case, we are adding real-world topography that is based on the ETOPO5 dataset (NOAA, 1988). The original topography is limited to positive values only, and scaled by a factor 0.5 to ensure that topography is covered by the fluid at all times. We run the model at a 5.6° model resolution (64×32 grid-points). The timestep length is chosen to be $240s$, which satisfies the Courant number requirement of the chosen discretisation. We choose a comparably small ϵ value of $1 \cdot 10^{-10}$ to study convergence of the solver over a wide dynamic range. The model is run for 120 days. Figure 1 is showing snapshots of the model state. Due to interactions with the topography, the initial zonal jet structure is decaying, leading to an abundance of different flow states and scales.

2.3 The Machine-Learned Preconditioner

It is the task of a preconditioner \mathcal{P} to reduce the overall workload required by the solver. The preconditioner achieves this by providing an estimate of the solution error $\mathcal{P}^{-1}(r_\nu) \approx \mathcal{L}^{-1}(r_\nu) = \Phi^{n+1} - \Phi_\nu$, the increment to the fluid thickness Φ_ν that is re-

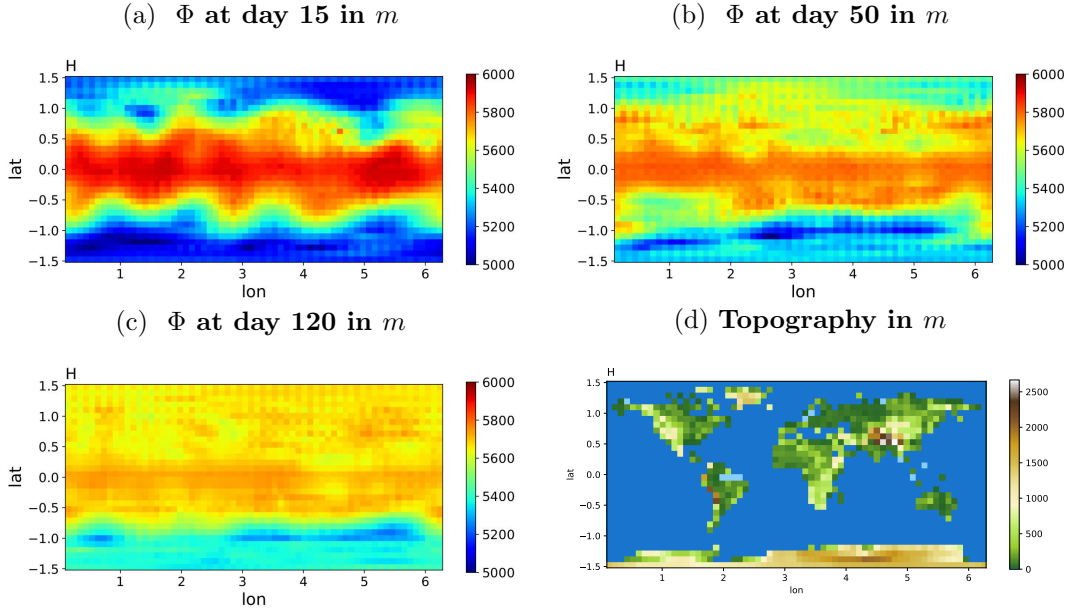


Figure 1. Snapshots of fluid thickness Φ in [m] after 15 (a), 50 (b), 120 (c) simulation days, as well as the model topography in [m] (d). Latitude and longitude are in radians.

quired to reach the next timestep Φ^{n+1} . We therefore train our machine-learned preconditioners to predict an estimate $\Delta\tilde{\Phi}$ of the required increment $\Delta\Phi := \Phi^{n+1} - \Phi^n$.

As the machine-learning tool of choice, we use fully-connected, feed-forward, neural networks. For these networks, the value of the i -th neuron of the k -th hidden layer $y_i^{(k)}$ is the result of applying an activation function ϕ to the weighted sum of outputs $y_j^{(k-1)}$ from the previous layer $k - 1$:

$$y_i^{(k)} = \phi \left(\sum_{j=0}^{m_{k-1}} w_j^{(k, i)} y_j^{(k-1)} + b_k \right),$$

where m_{k-1} is the number of neurons in layer $k - 1$, $w^{(k, i)}$ is the vector of weights of the i -th neuron of layer k , and b_k is a bias term. For the hidden layers, the ReLU activation function $\phi_{ReLU}(x) := \max(0, x)$ provided the best results. We use a linear activation function for the output layer.

We set up the neural network to predict a single grid-point value of $\Delta\tilde{\Phi}$ at a time. The input is based on grid stencils of the 6 coefficients (A^{ij} and B^i) of the linear operator \mathcal{L} (which are constant throughout the timestep) plus the residual r_ν . We normalize the six coefficient fields to stay in the interval $[-0.5, 0.5]$. Motivated by the linearity of operator \mathcal{L} , the input residual values r_ν and output values $\Delta\tilde{\Phi}$ are rescaled via division by $2 \|r_\nu\|_\infty$. This rescaling aims at making the machine-learned preconditioner invariant to the shrinking dynamical range of residual values r_ν over subsequent solver iterations.

Reminiscent of local approximate inverse preconditioners (Smith et al., 1992), we use '3×3' and '5×5' stencils of the input fields to predict $\Delta\tilde{\Phi}$ for the grid-point in the

centre. A 5×5 stencil that predicts $\Delta\tilde{\Phi}$ at grid-point i, j uses the following set of grid indices

$$\{(k, l) : k = i - 2, \dots, i + 2; l = j - 2, \dots, j + 2\}$$

for all input fields. Near the poles, the stencil is completed by continuing the meridians over the poles – in accordance with the underlying discretisation.

For the training and validation sets, we use data of the first solver iteration from the 120 day reference simulation. We train a neural network for each latitudinal band separately. To make sure that the training and validation data-sets are sufficiently independent, we built them as follows: The initial 14 days of model integration time are omitted to avoid potential shocks in the data from initialization. Afterwards, the data is split into cycles of three weeks of integration time. For each of the three week cycles, we use all timesteps from days 1–14 for training, omit day 15, use all timesteps from days 16–20 for validation, and omit day 21. This results in $1.6 \cdot 10^6$ training samples and $6 \cdot 10^5$ validation samples for each latitude.

Neural networks of different sizes are trained and tested. The neural network size ranges from 5 hidden layers and 200 neurons per layer (L5N200) to 1 hidden layer with 5 neurons (L1N5). However, we also tested a linear regression model (L0N0). All neural networks are implemented in Keras (Chollet et al., 2015) and trained using the Adam stochastic optimization (Kingma & Ba, 2014; Reddi et al., 2019). The loss function is the mean-squared-error (MSE) metric. The neural networks are trained for at least 50 epochs, with a batch size of 32.

3 Results

3.1 Offline Performance of the Machine-Learned Preconditioners

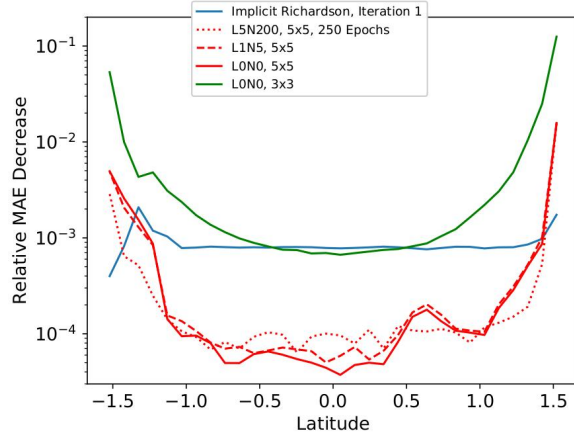
To get a first impression about the quality of results, we compare the relative decrease in Mean Absolute Error (MAE) at each latitude for the first iteration of the solver between the simulation using the implicit Richardson and the Neural Network preconditioner in Figure 2(a). Lower values mean better performance, i.e. higher error reduction.

In the first solver iteration, the implicit Richardson preconditioner manages a relative decrease in MAE of 3 orders of magnitude. As expected, by design this type of preconditioner does a good job at providing stable performance near the poles despite the poleward grid convergence.

In comparison, the 5×5 stencil machine-learned preconditioners achieve a relative decrease in MAE of $2 \cdot 10^{-2}$ and $5 \cdot 10^{-3}$ near the North- and South-poles respectively. The machine-learning preconditioners performs even better equatorwards where they achieve a relative reduction in MAE of up to $5 \cdot 10^{-5}$. Surprisingly, the size of the neural network has no significant impact. The L5N200 preconditioner is not consistently better than the L0N0 preconditioner. At the same time, the L5N200 preconditioner needed an increased number of 250 epochs for convergence. Using other activation functions for the L5N200 neural network such as *tanh* does not improve results (not shown here).

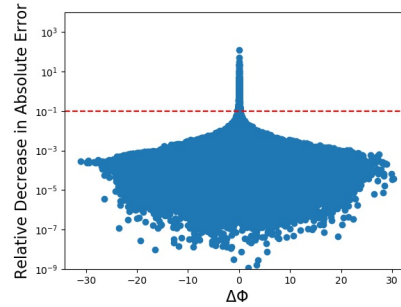
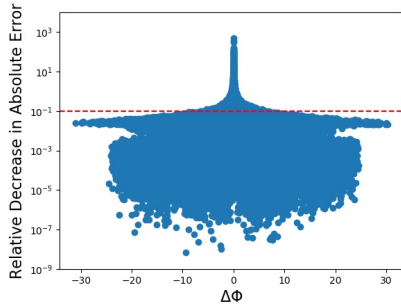
As the L0N0 preconditioner will be the cheapest machine-learning preconditioner, the L0N0 with a 5×5 stencil can be considered the most promising option. To complete our analysis, we train a L0N0 preconditioner on the smaller 3×3 stencil. Although behaving qualitatively similar to the L0N0, 5×5 preconditioner, it consistently performs worse by about one order of magnitude at all latitudes.

(a) Comparison of different machine-learned Preconditioners



(b) L0N0, 5×5

(c) Implicit Richardson



(d) L0N0, 5×5 , Relative Contributions
of the r_0 Input Stencil

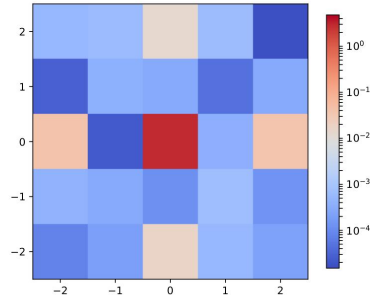


Figure 2. a) Relative decrease in Mean Absolute Error (MAE) as a function of latitude for the validation set for the implicit Richardson Preconditioner in comparison to neural networks of various sizes and input stencil widths. b) and c) show the absolute values of $\frac{\Delta\tilde{\Phi}-\Delta\Phi}{\Delta\Phi}$ as a function of $\Delta\Phi$ for the zonal band closest to the South pole for b) the L0N0, 5×5 preconditioner, and c) the implicit Richardson preconditioner. d) shows the mean absolute of relative contributions of the residual r_0 input stencil towards the error prediction $\Delta\tilde{\Phi}$ of the L0N0, 5×5 preconditioner at latitude $\phi = 1.03$ ($59^\circ N$).

To better understand the structure of the relative errors and whether the machine-learning preconditioners behave robustly, we further analyze the behavior of the L0N0, 5×5 preconditioner. We show the absolute values of relative error $\frac{\Delta\tilde{\Phi}-\Delta\Phi}{\Delta\Phi}$ as a function of $\Delta\Phi$ for the first solver iteration in Figure 2 (b) and (c) for the L0N0, 5×5 and the implicit Richardson preconditioner. The data shown is for the zonal band closest to the South Pole, the qualitative results are the same for the other latitudes (not shown here).

The L0N0, 5×5 preconditioner and the implicit Richardson preconditioner share the same qualitative behaviour. For a large range of $\Delta\Phi$ values, both preconditioners are good and robust predictors and reduce $\Delta\Phi$ by at least one order of magnitude (red, horizontal line). The reduction per preconditioner application is larger for the implicit Richardson preconditioner. Only for very small values of $\Delta\Phi$, we find that applying the preconditioner actually increases the error. This occurs for both preconditioners and is simply a reminder that the task of preconditioning is inherently a problem of making a prediction with incomplete information.

3.2 Online Performance of the Machine-learned Preconditioner

We now use the L0N0, 5×5 preconditioner within free-running simulations of the shallow-water model. For our first convergence test, we use the L0N0, 5×5 preconditioner and run a simulation until day 120. To rule out the possibility that our machine-learned preconditioner is only valid for one specific flow trajectory (assuming that the pre-chosen solver accuracy is so high that it results in the same trajectory), we show the L0N0, 5×5 preconditioner results from a simulation where initial conditions for the momentum Q_x are stochastically perturbed by 5% of their value. The perturbed and unperturbed runs slowly decorrelate, the correlation coefficient for Q_y after 50 days is down to 0.44. Note that, the L0N0, 5×5 preconditioner is used for all solver iterations and we thus go beyond the training and validation data that only used data from the first solver iteration. The convergence rate using the L0N0, 5×5 preconditioner (Figure 3 (a)) is almost doubled compared to running the model without a preconditioner (Figure 3 (c)) for all iterations but almost halved when compared to the implicit Richardson preconditioner (Figure 3 (b)).

This convergence behavior is also found for the first 15 days of integration time of the test-case – the initial spin-up phase – which lies outside of the training data, see Figures 3 (d) and 3 (e).

The L0N0, 5×5 preconditioner thus consistently increases the convergence rate of the linear solver in different scenarios that were not part of the training data.

3.2.1 Interpretability of the Machine-learned Preconditioner

Because of the low complexity of the L0N0, 5×5 preconditioner – please note that L0N0 is equivalent to the use of linear regression – we can dissect how each input contributes towards the final prediction $\Delta\tilde{\Phi}$. We show the mean absolute relative contribution of the residuals r_0 input stencil in Figure 2 (d). Here, we only show the contribution for latitude $59^\circ N$. However, results are qualitatively the same for the other latitudes.

In the contributions of the residuals r_0 (Figure 2 (d)), the underlying stencil of the generalized Laplace operator \mathcal{L} in equation (7) shines through. We see 5 dominant values: two in zonal direction, two in meridional direction, and the center-most grid-point. The center-most grid-point value has the largest contribution and represents the inversion of the main diagonal terms.

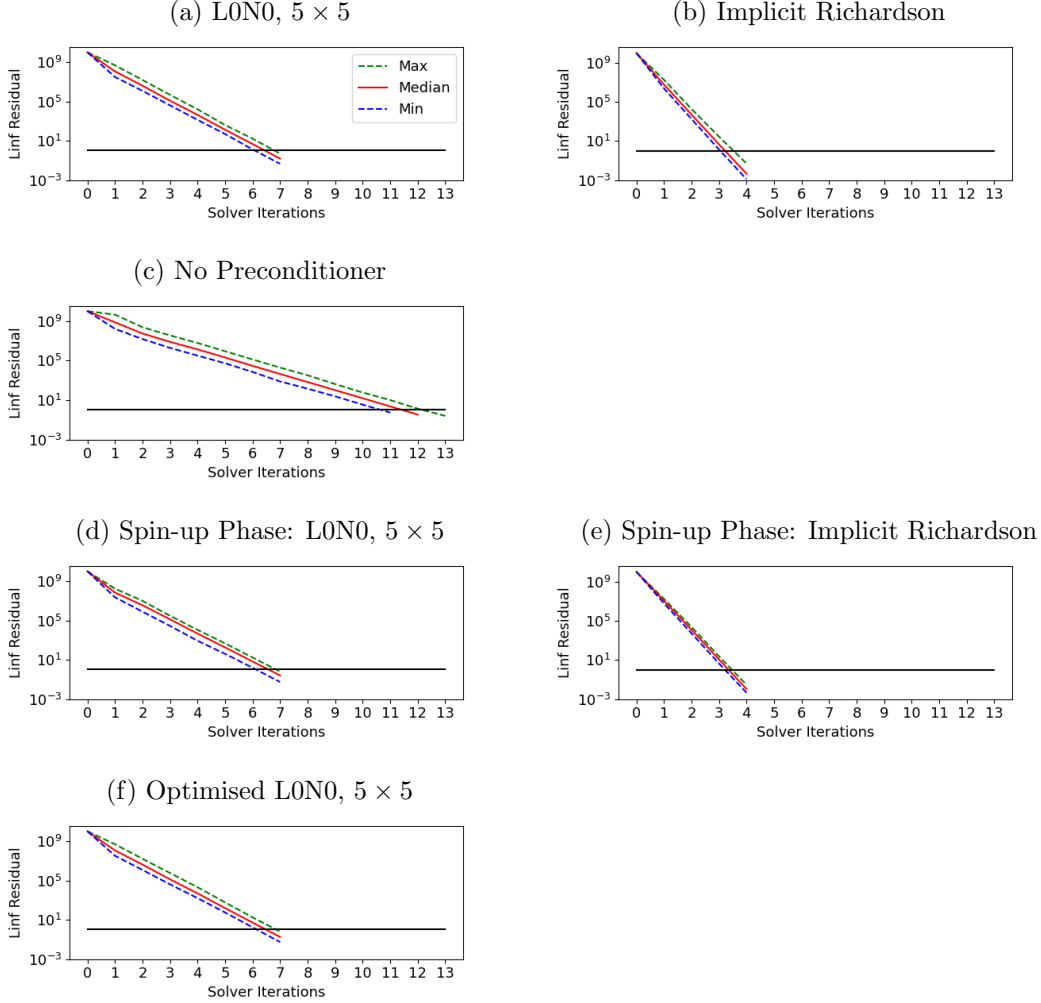


Figure 3. Convergence rate analysis of the linear solvers for the implicit Richardson preconditioner and the L0N0, 5×5 preconditioner. The shown maxima, minima, and median values of the residual norms $\|r_\nu\|_\infty$ are normalized by $\epsilon \|r_0\|_\infty$. The convergence rate of the L0N0, 5×5 preconditioner for days 15-120 is shown in (a), this simulation is run from perturbed initial conditions (initial fields are randomly perturbed by 5%). Respective convergence rates using the implicit Richardson preconditioner and no preconditioner are shown in (b) and (c), respectively. For days 0-15, the performance of the L0N0, 5×5 preconditioner is shown in (d), with the respective implicit Richardson reference given in (e). In (f), we show the same information as in (a) for the optimised version of the L0N0, 5×5 preconditioner (see Section 3.2.1).

The contributions of the coefficients A^{ij} and B^i (see supporting information) are found potentially negligible as they contribute less than 2.5% to the total of the final prediction values of $\Delta\Phi$.

Thus, we train an optimised version of the L0N0, 5×5 preconditioner that only uses the residuals r_ν as inputs. As most of these residual inputs within the stencil have negligible contributions as well, we further restrict the L0N0, 5×5 preconditioner input and use only data from local stencil coordinates $(0, 2)$, $(-2, 0)$, $(0, 0)$, $(2, 0)$, and $(0, -2)$ (with $(0, 0)$ being the centre of the stencil). The resulting model simulation with the “op-

timised” L0N0 preconditioner which is using only five input values performs as well as the standard version, see Figure 3 (f).

3.3 Performance Estimates

To compare the overall efficiency of the solvers, the computational overhead of the preconditioners needs to be taken into account. In a sequential setting and small problem sizes, a simple analysis of the required floating-point operations is a good performance model for the preconditioned linear solvers.

The optimised L0N0, 5×5 preconditioner requires almost twice as many solver iterations for the same accuracy compared to the implicit Richardson preconditioner. However, each application of the machine-learned preconditioner (10 floating-point operations per grid-point) is 4 times cheaper than the implicit Richardson preconditioner (38 floating-point operations). In summary, including the rest of the elliptic solver steps + solver and preconditioner initialisation, both preconditioners result in the same computational saving of about 30 percent over the unpreconditioned elliptic solver.

4 Discussion and Conclusion

We show a proof-of-concept for the derivation of a machine-learned preconditioner in a representative shallow-water model. The machine-learned preconditioner performs equally well as the implicit Richardson preconditioner that was used as a reference. This is a positive result that shows the great potential of our approach. In fact, it is rather surprising that a very simple machine learning solution – which is basically using simple linear regression – is already sufficient to perform so efficiently for a two-dimensional fluid problem.

The performance estimates that were presented in this paper will likely not hold for larger problem sizes and supercomputing environments. Here, performance will mostly be limited by data movement rather than floating point arithmetic. However, machine-learned preconditioners have clear advantages when compared with a conventional preconditioner as they are based on local grid stencils whose shape and size can be flexibly chosen and optimised to yield the best performance on any given hardware system. Furthermore, deep learning applications can make very efficient use of modern hardware since they are based on dense linear algebra. The use of reduced numerical precision may help to further reduce the cost of machine-learned preconditioners.

The test configuration discussed in this paper is still simple when compared to the complexity of the task to develop efficient preconditioners for high-resolution, three-dimensional atmosphere or ocean models, mainly due to the stiffness caused by vertical grid spacing of as little as a couple of meters close to the surface. However, as the power of deep learning to learn complex non-linear relationships with complex neural networks was not even required for the shallow water model, we are optimistic that machine learning preconditioners will perform well for three-dimensional models. Also, our approach might not be limited just to preconditioners because smoothers for multigrid solvers might be derived in a very similar fashion.

Acknowledgments

Jan Ackmann and Tim Palmer were funded via the European Research Council project ITHACA (grant No. 741112). Peter Dueben gratefully acknowledges funding from the Royal Society for his University Research Fellowship. Peter Dueben and Piotr Smolarkiewicz received funding from the ESiWACE and ESiWACE2 projects. ESiWACE and ESiWACE2 have received funding from the European Union’s Horizon 2020 research and innovation programme under grant agreement No 675191 and 823988. NCAR is sponsored by the

National Science Foundation. We would like to thank Christian Kuehnlein for many helpful discussions. All source code can be found in repository: <https://github.com/JanAckmann/MLPrecon>.

References

- Chevallier, F., Chéruy, F., Scott, N. A., & Chédin, A. (1998). A neural network approach for a fast and accurate computation of a longwave radiative budget. *Journal of Applied Meteorology*, *37*(11), 1385–1397. Retrieved from [https://doi.org/10.1175/1520-0450\(1998\)037<1385:ANNAFA>2.0.CO;2](https://doi.org/10.1175/1520-0450(1998)037<1385:ANNAFA>2.0.CO;2); doi: 10.1175/1520-0450(1998)037<1385:ANNAFA>2.0.CO;2
- Chollet, F., et al. (2015). *Keras*. <https://keras.io>.
- Dedner, A., Müller, E., & Scheichl, R. (2016). Efficient multigrid preconditioners for atmospheric flow simulations at high aspect ratio. *International Journal for Numerical Methods in Fluids*, *80*(1), 76–102. doi: 10.1002/fld.4072
- Dueben, P. D., & Bauer, P. (2018, oct). Challenges and design choices for global weather and climate models based on machine learning. *Geoscientific Model Development*, *11*(10), 3999–4009. doi: 10.5194/gmd-11-3999-2018
- Eisenstat, S. C., Elman, H. C., & Schultz, M. H. (1983). Variational iterative methods for nonsymmetric systems of linear equations. *SIAM Journal on Numerical Analysis*, *20*(2), 345–357.
- Fuhrer, O., Chadha, T., Hoefler, T., Kwasniewski, G., Lapillonne, X., Leutwyler, D., ... Vogt, H. (2018). Near-global climate simulation at 1 km resolution: establishing a performance baseline on 4888 GPUs with COSMO 5.0. *Geoscientific Model Development*, *11*(4), 1665–1681. Retrieved from <https://www.geosci-model-dev.net/11/1665/2018/>; doi: 10.5194/gmd-11-1665-2018
- Gentine, P., Pritchard, M., Rasp, S., Reinaudi, G., & Yacalis, G. (2018). Could machine learning break the convection parameterization deadlock? *Geophysical Research Letters*, *45*(11), 5742–5751. Retrieved from <https://agupubs.onlinelibrary.wiley.com/doi/abs/10.1029/2018GL078202>; doi: 10.1029/2018GL078202
- George, T., Gupta, A., & Sarin, V. (2008, Dec). A recommendation system for preconditioned iterative solvers. In *2008 eighth ieee international conference on data mining* (p. 803–808). doi: 10.1109/ICDM.2008.105
- Götz, M., & Anzt, H. (2018). Machine learning-aided numerical linear algebra: Convolutional neural networks for the efficient preconditioner generation. In *2018 ieee/acm 9th workshop on latest advances in scalable algorithms for large-scale systems (scala)* (pp. 49–56).
- Holloway, A., & Chen, T.-Y. (2007). Neural networks for predicting the behavior of preconditioned iterative solvers. In *International conference on computational science* (pp. 302–309).
- Huang, Z., England, M., Davenport, J. H., & Paulson, L. C. (2016, Sep.). Using machine learning to decide when to precondition cylindrical algebraic decomposition with groebner bases. In *2016 18th international symposium on symbolic and numeric algorithms for scientific computing (synasc)* (p. 45–52). doi: 10.1109/SYNASC.2016.020
- Kingma, D. P., & Ba, J. (2014). Adam: A method for stochastic optimization. *arXiv preprint arXiv:1412.6980*.
- Krasnopolsky, V. M., Fox-Rabinovitz, M. S., Hou, Y. T., Lord, S. J., & Belochitski, A. A. (2010). Accurate and fast neural network emulations of model radiation for the ncep coupled climate forecast system: Climate simulations and seasonal predictions. *Monthly Weather Review*, *138*(5), 1822–1842. doi: 10.1175/2009MWR3149.1
- Kuefler, E., & Chen, T.-Y. (2008). On using reinforcement learning to solve sparse linear systems. In *International conference on computational science* (pp. 955–

- 964).
- Kühnlein, C., Deconinck, W., Klein, R., Malardel, S., Piotrowski, Z. P., Smolarkiewicz, P. K., ... Wedi, N. P. (2019, feb). FVM 1.0: a nonhydrostatic finite-volume dynamical core for the IFS. *Geoscientific Model Development*, 12(2), 651–676. Retrieved from <https://www.geosci-model-dev.net/12/651/2019/> doi: 10.5194/gmd-12-651-2019
- Kurth, T., Treichler, S., Romero, J., Mudigonda, M., Luehr, N., Phillips, E., ... et al. (2018). Exascale deep learning for climate analytics. In *Proceedings of the international conference for high performance computing, networking, storage, and analysis*. IEEE Press.
- Ladický, L., Jeong, S., Solenthaler, B., Pollefeys, M., & Gross, M. (2015, October). Data-driven fluid simulations using regression forests. *ACM Trans. Graph.*, 34(6). Retrieved from <https://doi.org/10.1145/2816795.2818129> doi: 10.1145/2816795.2818129
- Maynard, C., Melvin, T., & Müller, E. H. (2020). *Multigrid preconditioners for the mixed finite element dynamical core of the LFRic atmospheric model*.
- Mengaldo, G., Wyszogrodzki, A., Diamantakis, M., Lock, S.-J., Giraldo, F. X., & Wedi, N. P. (2019, JUL). Current and Emerging Time-Integration Strategies in Global Numerical Weather and Climate Prediction [Review]. *ARCHIVES OF COMPUTATIONAL METHODS IN ENGINEERING*, 26(3), 663-684. doi: {10.1007/s11831-018-9261-8}
- Müller, E. H., & Scheichl, R. (2014). Massively parallel solvers for elliptic partial differential equations in numerical weather and climate prediction. *Quarterly Journal of the Royal Meteorological Society*, 140(685), 2608-2624. Retrieved from <https://rmets.onlinelibrary.wiley.com/doi/abs/10.1002/qj.2327> doi: 10.1002/qj.2327
- NOAA, N. G. D. C. (1988). Data announcement 88-mgg-02, digital relief of the surface of the earth.
- Palmer, T., & Stevens, B. (2019). The scientific challenge of understanding and estimating climate change. *Proceedings of the National Academy of Sciences*, 116(49), 24390–24395. Retrieved from <https://www.pnas.org/content/116/49/24390> doi: 10.1073/pnas.1906691116
- Peairs, L., & Chen, T.-Y. (2011). Using reinforcement learning to vary the m in gmres(m). *Procedia Computer Science*, 4, 2257 - 2266. Retrieved from <http://www.sciencedirect.com/science/article/pii/S1877050911003048> (Proceedings of the International Conference on Computational Science, ICCS 2011) doi: <https://doi.org/10.1016/j.procs.2011.04.246>
- Piotrowski, Z. P., Matejczyk, B., Marcinkowski, L., & Smolarkiewicz, P. K. (2016). Parallel adi preconditioners for all-scale atmospheric models. In R. Wyrzykowski, E. Deelman, J. Dongarra, K. Karczewski, J. Kitowski, & K. Wiatr (Eds.), *Parallel processing and applied mathematics* (pp. 607–618). Cham: Springer International Publishing.
- Prusa, J. M., Smolarkiewicz, P. K., & Wyszogrodzki, A. A. (2008, oct). EULAG, a computational model for multiscale flows. *Computers & Fluids*, 37(9), 1193–1207. Retrieved from <https://www.sciencedirect.com/science/article/abs/pii/S004579300700206X> doi: 10.1016/J.COMPFLUID.2007.12.001
- Rasp, S., Pritchard, M. S., & Gentine, P. (2018). Deep learning to represent sub-grid processes in climate models. *ArXiv e-prints*.
- Reddi, S. J., Kale, S., & Kumar, S. (2019). On the convergence of adam and beyond. *arXiv preprint arXiv:1904.09237*.
- Rizzuti, G., Siahkoohi, A., & Herrmann, F. (2019). Learned iterative solvers for the helmholtz equation. , 2019(1), 1-5. Retrieved from <https://www.earthdoc.org/content/papers/10.3997/2214-4609.201901542> doi: <https://doi.org/10.3997/2214-4609.201901542>
- Scher, S., & Messori, G. (2019, mar). Weather and climate forecasting with neu-

- ral networks: using GCMs with different complexity as study-ground. *Geoscientific Model Development Discussions*, 1–15. doi: 10.5194/gmd-2019-53
- Schneider, T., Lan, S., Stuart, A., & Teixeira, J. (2018). Earth system modeling 2.0: A blueprint for models that learn from observations and targeted high-resolution simulations. *Geophysical Research Letters*. doi: 10.1002/2017GL076101
- Smith, R., Dukowicz, J., & Malone, R. (1992). Parallel ocean general circulation modeling. *Physica D: Nonlinear Phenomena*, 60(1), 38 - 61. Retrieved from <http://www.sciencedirect.com/science/article/pii/016727899290225C> doi: [https://doi.org/10.1016/0167-2789\(92\)90225-C](https://doi.org/10.1016/0167-2789(92)90225-C)
- Smolarkiewicz, P., & Margolin, L. (2000). *Variational methods for elliptic problems in fluid models* (Tech. Rep.). Los Alamos National Lab., NM (US).
- Smolarkiewicz, P. K., Deconinck, W., Hamrud, M., Kühnlein, C., Mozdzyński, G., Szmelter, J., & Wedi, N. P. (2016). A finite-volume module for simulating global all-scale atmospheric flows. *Journal of Computational Physics*. doi: 10.1016/j.jcp.2016.03.015
- Smolarkiewicz, P. K., Kühnlein, C., & Wedi, N. P. (2019, jan). Semi-implicit integrations of perturbation equations for all-scale atmospheric dynamics. *Journal of Computational Physics*, 376, 145–159. Retrieved from <https://www.sciencedirect.com/science/article/pii/S002199911830634X> doi: 10.1016/J.JCP.2018.09.032
- Smolarkiewicz, P. K., & Margolin, L. G. (1998). *MPDATA: A Finite-Difference Solver for Geophysical Flows*. doi: 10.1006/jcph.1998.5901
- Szmelter, J., & Smolarkiewicz, P. K. (2010). An edge-based unstructured mesh discretisation in geospherical framework. *Journal of Computational Physics*, 229(13), 4980 - 4995. Retrieved from <http://www.sciencedirect.com/science/article/pii/S0021999110001270> doi: <https://doi.org/10.1016/j.jcp.2010.03.017>
- Tompson, J., Schlachter, K., Sprechmann, P., & Perlin, K. (2017). Accelerating eulerian fluid simulation with convolutional networks. In *Proceedings of the 34th international conference on machine learning-volume 70* (pp. 3424–3433).
- Weyn, J. A., Durran, D. R., & Caruana, R. (2019). Can machines learn to predict weather? using deep learning to predict gridded 500-hpa geopotential height from historical weather data. *Journal of Advances in Modeling Earth Systems*, 11(8), 2680-2693. Retrieved from <https://agupubs.onlinelibrary.wiley.com/doi/abs/10.1029/2019MS001705> doi: 10.1029/2019MS001705
- Williamson, D. L., Drake, J. B., Hack, J. J., Jakob, R., & Swarztrauber, P. N. (1992). A standard test set for numerical approximations to the shallow water equations in spherical geometry. *Journal of Computational Physics*, 102, 211 - 224. Retrieved from <https://www.sciencedirect.com/science/article/pii/S0021999105800166>
- Xu, S., & Zhang, J. (2005). A data mining approach to matrix preconditioning problem. In *Proceedings of the eighth workshop on mining scientific and engineering datasets (msd05)*.
- Yamada, K., Katagiri, T., Takizawa, H., Minami, K., Yokokawa, M., Nagai, T., & Ogino, M. (2018, Nov). Preconditioner auto-tuning using deep learning for sparse iterative algorithms. In *2018 sixth international symposium on computing and networking workshops (candarw)* (p. 257-262). doi: 10.1109/CANDARW.2018.00055
- Yang, C., Xue, W., Fu, H., You, H., Wang, X., Ao, Y., ... Zheng, W. (2016, Nov). 10m-core scalable fully-implicit solver for nonhydrostatic atmospheric dynamics. In *Sc '16: Proceedings of the international conference for high performance computing, networking, storage and analysis* (p. 57-68). doi: 10.1109/SC.2016.5
- Yang, C., Yang, X., & Xiao, X. (2016). Data-driven projection method in fluid simu-

lation. *Computer Animation and Virtual Worlds*, 27(3-4), 415-424. Retrieved from <https://onlinelibrary.wiley.com/doi/abs/10.1002/cav.1695> doi: 10.1002/cav.1695

Supporting Information for ”Machine-Learned Preconditioners for Linear Solvers in Geophysical Fluid Flows”

Jan Ackmann¹, Peter D. Düben², Tim N. Palmer¹, Piotr K. Smolarkiewicz³

¹University of Oxford, Oxford, OX1 3PU, UK

²European Centre For Medium Range Weather Forecasts, Reading, RG2 9AX, UK

³National Center for Atmospheric Research, Boulder, CO 80026, USA

Contents of this file

1. Text S1
2. Figure S1 to S2

Introduction In this supplementary information file, the reference implicit Richardson preconditioner is described in more detail in Text S1. Figure S1 is a flowchart of the Generalized Conjugated Residual method (GCR) that was used in this publication. Figure S2 provides additional information on the contributions from the input stencils of the linear operator for the L0N0, 5×5 preconditioner.

Text S1. Implicit Richardson based Preconditioner

The implicit Richardson preconditioner obtains an estimate of the solution error $\mathcal{P}^{-1}(r_{\nu+1}) \approx \mathcal{L}^{-1}(r_{\nu+1})$ by means of a stationary iteration, indexed with μ and initialized with $q_0 = 0$ — best described as a semi-implicit Richardson scheme. For this, the operator is split into two parts. The first part combines the second-order zonal derivative term and the Helmholtz term, $\mathcal{P}^{\mathcal{Z}} + \mathcal{P}^{\mathcal{H}}$. The second part, denoted by $\mathcal{P}^{\mathcal{M}}$, consists of the second-order meridional derivative term. In the semi-implicit Richardson scheme, the first part is then taken at iteration $\mu + 1$ while the second part is lagged behind. This results in a tridiagonal problem

$$\left[I - \eta \mathcal{P}^{\mathcal{Z}} - \eta \mathcal{P}^{\mathcal{H}} \right] q_{\mu+1} = q_{\mu} + \eta \left[\mathcal{P}^{\mathcal{M}} q_{\mu} - r_{\nu+1} \right], \quad (1)$$

where I denotes the identity operator, and η can be interpreted as a pseudotimestep, determined from linear stability theory for the $\mathcal{P}^{\mathcal{M}}$ operator. In our experiments, we find that performing only one iteration yields the best overall performance.

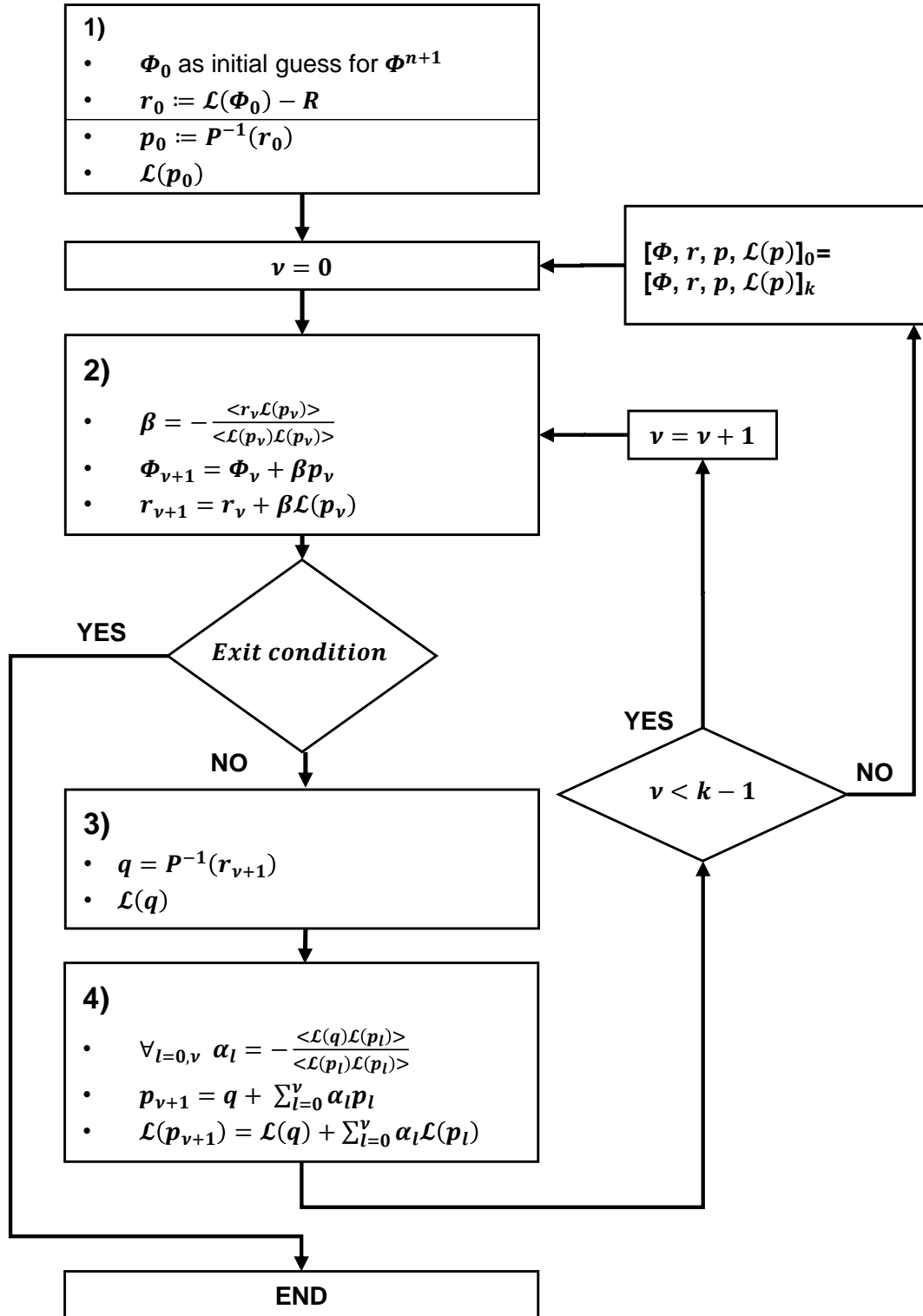


Figure S1. We show a flow chart of the generalized Conjugated Residual method GCR(k) that is implemented for this work (here $k = 1$)

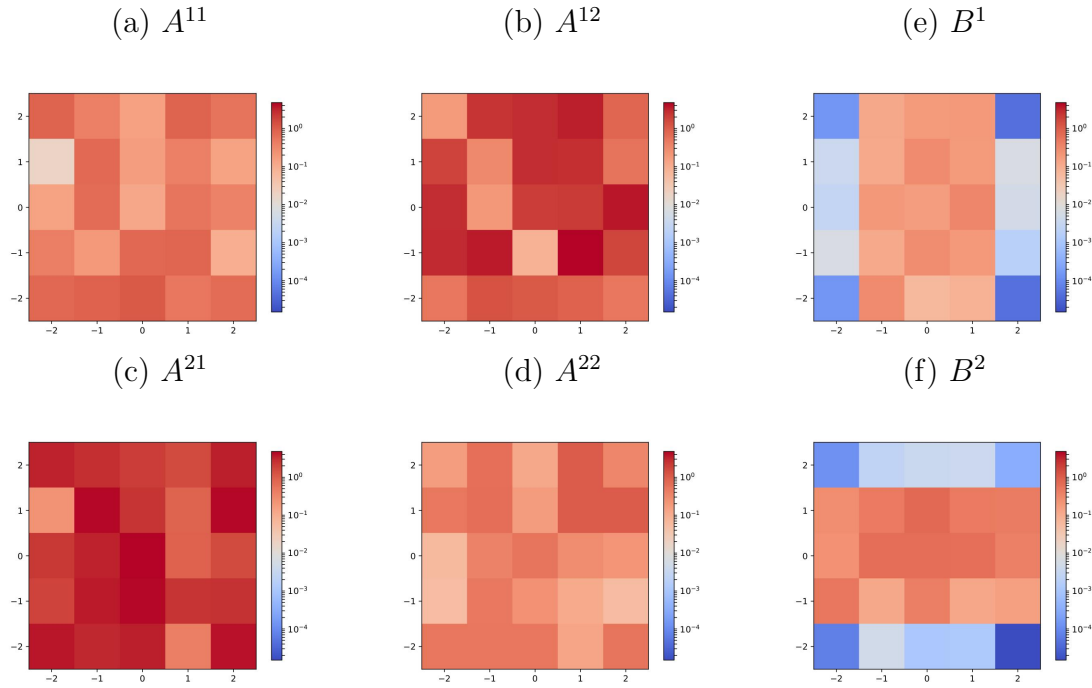


Figure S2. Mean absolute relative contribution of input fields towards the error prediction $\Delta\tilde{\Phi}$ for latitude $\phi = 1.03$ ($59^\circ N$). The plots show the 5×5 stencil of the two-dimensional fields to precondition the grid-point in the centre. a), b), c), and d) show the contribution of the components of A^{11} , A^{12} , A^{21} , and A^{22} respectively. e), f) show the contribution of the components of B^1 , and B^2 .